Scanning Microscopy

Volume 1993
Number 7 *Physics of Generation and Detection of Signals Used for Microcharacterization*

Article 16

1993

Applications of Charge Collection Microscopy: Electron-Beam-Induced Current to Semiconductor Materials and Device Research

Richard J. Matson
National Renewable Energy Laboratory, Colorado

Follow this and additional works at: https://digitalcommons.usu.edu/microscopy

Part of the Biology Commons

Recommended Citation

Matson, Richard J. (1993) "Applications of Charge Collection Microscopy: Electron-Beam-Induced Current to Semiconductor Materials and Device Research," *Scanning Microscopy*: Vol. 1993 : No. 7 , Article 16.
Available at: https://digitalcommons.usu.edu/microscopy/vol1993/iss7/16

This Article is brought to you for free and open access by the Western Dairy Center at DigitalCommons@USU. It has been accepted for inclusion in Scanning Microscopy by an authorized administrator of DigitalCommons@USU. For more information, please contact digitalcommons@usu.edu.

Scanning Microscopy Supplement 7, 1993 (Pages 243-251)
Scanning Microscopy International, Chicago (AMF O'Hare), IL 60666 USA

0892-953X/93$5.00+.25

APPLICATIONS OF CHARGE COLLECTION MICROSCOPY: ELECTRON-BEAM-INDUCED CURRENT TO SEMICONDUCTOR MATERIALS AND DEVICE RESEARCH

Richard J. Matson

National Renewable Energy Laboratory
1617 Cole Blvd., Golden, CO 80401
Phone No.: (303) 275-3726, FAX No.: (303) 275-3701

Abstract

Among all of the possible techniques for the micro-characterization of semiconductor materials and devices in a scanning electron microscope (SEM), charge collection microscopy (CCM), more commonly known as electron-beam-induced current (EBIC), is probably both the most easily deployed and the most versatile characterization technique. Following a brief review of the basic theory of the generation and detection of the EBIC signals, various techniques and applications to the micro-characterization of experimental semiconductor materials and devices will be presented. The applications are primarily to emerging photovoltaic materials and devices. This report is not in any way intended as a complete overview of all EBIC related techniques or most material or device applications. Beyond offering a short review of CCM theory, this paper complements the literature (1) as a basic introduction to CCM, and (2) by focusing on the use and extension of CCM techniques for basic studies in experimental electronic materials.

Key Words: Charge collection microscopy (CCM), electron-beam-induced current (EBIC), micro-characterization, photovoltaic, introduction.

Introduction

The many ways in which a high energy electron interacts with matter give rise to a number of useful, observable signatures of a sample in the scanning electron microscope (SEM). Semiconducting materials and devices, in particular, lend themselves to a wide variety of SEM-based analytical approaches. In particular: charge collection microscopy (CCM), voltage contrast (VC), cathodoluminescence (CL), electron channeling (EC), scanning deep-level transient spectroscopy (SDLTS), and scanning electron-acoustic (thermal wave) microscopy (SEAM). All of these have been reviewed in the book SEM Micro-Characterization of Semiconductors, edited by D.B. Holt and D.C. Joy (1989). Of all of these microcharacterization techniques, CCM may be the most easily deployed and the most powerful analytical tool for characterizing electronic materials and devices. As a practical introduction, it is the purpose of the present paper to briefly review the theory of the generation and detection of the CCM/EBIC (electron-beam-induced current) signal and then present a variety of recent extensions and applications of EBIC techniques. The terms EBIC and CCM will be used interchangeably in this paper because EBIC is the most commonly used term for this technique in the literature and in the community, although "EBIC" can be confused with electron-beam-induced conductivity and is thereby less precise than CCM (see Holt, 1974). Charge collection has also been called the barrier electron voltaic effect and is the least commonly used term in the literature (Ehrenberg *et al.*, 1981; Leamy, 1982; Holt, 1974; Holt, 1989).

Generation and Detection of EBIC Signal

When a semiconductor device is penetrated by energetic (>1 keV) primary electrons, the succession of scattering events, or "collisions," result in the promotion of electrons from the valence band to the conduction band, thereby producing electron-hole (e/h) pairs. Without the presence of an electric field, the electrons and holes simply recombine. If, as in the case of a

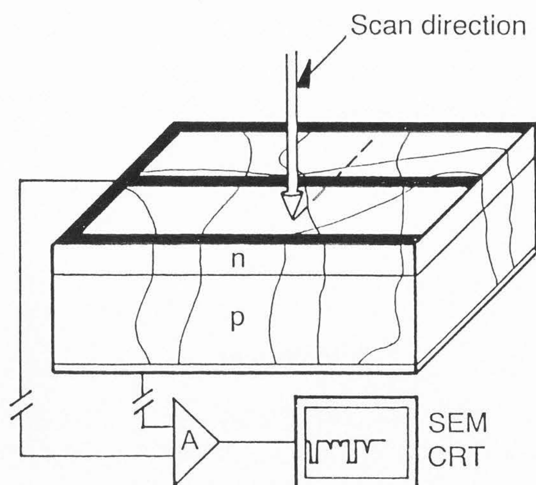

Figure 1. A schematic illustration of the scanning movement of an electron beam across a polycrystalline device. The light lines indicate grain boundaries which usually act as recombination sites and, therefore, locations of current loss.

semiconductor device, there is an electric field present within collection distance of the e/h creation, the electron and hole can be separated and collected via contacts to the device. In turn, this collected current is amplified and used to modulate the intensity of the SEM CRT (cathode ray tube), as indicated in Figure 1. As an example, an EBIC image (a) and a secondary electron image (SEI) (b) of a simple metal-insulator-semiconductor (MIS) device made from polycrystalline silicon is given in Figure 2. The effect of grain boundaries, or other sources of recombination, on the charge collection image is evident. Wherever there is electron/hole recombination, there is a corresponding loss of collected current and, therefore, CRT intensity, which appears as the dark areas in the image. Note the difference of the density of defects among different grains and differing portions of grain boundaries.

Essentially, the electron beam acts as a constant, mobile point source of current generation and can be used for "micro"-characterization, or characterization of micron scale variations in the electrical properties of a material or device.

Effectively, the sample itself is its own detector, and nothing other than amplification of the EBIC signal and a SEM vacuum chamber feedthrough for the signal is necessary to deploy this capability. Lacking an actual p-n junction in the device, the electric field required for charge separation can be provided through either an external bias applied to the device or through the simple fabrication of a Schottky barrier device. It is the

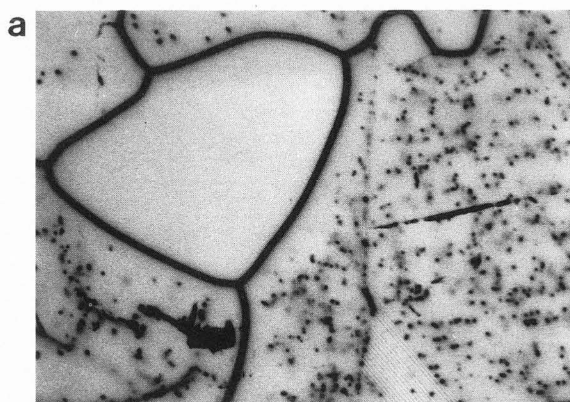

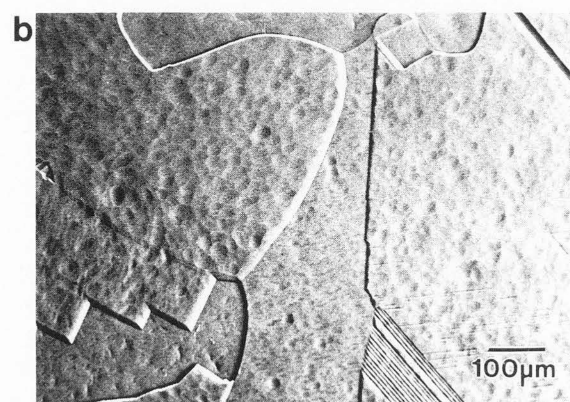

Figure 2. A comparison of an EBIC image (**a**) and the secondary electron image (SEI) (**b**) of the same area of a MIS device on Wacker polycrystalline silicon. The areas of recombination (defects) show up dark in EBIC images. Bar = 100 μm.

relative ease of creating such a Schottky barrier (often with the deposition of ~200 Å of Au) that readily extends the use of CCM to the investigation of developing electronic materials that are not yet devices.

Considering e^-/h^+ pair generation more closely, we can calculate ΔN, the number of e/h pairs generated per second for a given SEM beam condition, by

$$\Delta N = G\, I_b/q, \quad (1)$$

where

$$G = (1 - f)\, E_b/e_i, \quad (2)$$

and f is the average fraction of the energy of the incident beam electrons lost to back-scattering [often taken as half the backscatter coefficient (Holt, 1989)]; I_b and E_b are the electron beam current and voltage, respectively; q is the electronic charge; e_i is the ionization charge or the average energy required to create an e/h pair; and G is the gain. A good value for e_i is usually taken as

approximately three times the E_g of the material (Holt, 1989; Leamy, 1982). By dividing the energy available in a primary electron for ionization by the energy required for ionization, the gain, G, gives the factor by which the maximum EBIC can exceed the I_b, which commonly runs in the range of 10^3-10^4. The practical significance of this is (**a**) that common I_b values of 100 pA can give rise to μA-range signals which can be handled "cleanly" by most amplifiers, and (**b**) that even very inefficient experimental devices can still be characterized quite often by CCM. In this author's experience, the lowest "clean," or useful, scale for amplifiers is the nA scale. Hence, even a 1% efficient device and a 150-pA, 20-kV beam still leaves an adequate signal.

One use of the relation in equation (1) is to establish a reference for the efficiency of the device. Termed electron-beam quantum yield, or charge-collection efficiency of a barrier, η_{cc} (Holt, 1989), the measured EBIC, I_{cc}, is normalized to the theoretically generated current, or

$$\eta_{cc} = I_{cc} / GI_b. \quad (3)$$

This is demonstrated in Figure 3 on an epilayer of a GaAs-on-Si device where the atomic lattice mismatch resulted in dislocation networks. In Figure 3, the reference for 100% quantum efficiency (per equation 1) is represented by the top, horizontal line. The bottom line is both the position of the line scan and the zero beam current reference line. The middle line is the EBIC linescan indicating the actual current loss in a defect area relative to 100% collection. The EBIC linescan thereby indicates the degree of current-loss at those defects that are intersected by the EBIC linescan.

In addition to the amount of current that is being generated, or the number of carrier pairs injected, it is important to bear in mind their density and how they are spatially distributed. A common expression for the depth over which ionization occurs is given by the electron range, R_e (Leamy, 1982):

$$R_e(\mu m) = [(3.98*10^{-2})/\rho(g/cm^3)]*E_b(kV)^{1.75}, \quad (4)$$

where ρ is the density. Bearing in mind the nonuniform distribution of ionization activity, yet treating the generation volume as a sphere, R_e in diameter (Leamy, 1982; Holt, 1989), we note that the volume scales with R_e^3 and, therefore, with $E_b^{5.25}$. Hence, the energy density scales with $E_b^{-4.25}$ and halving the E_b increases the energy and ionization density by ~19. This bears directly on both entering the regime of high injection conditions (Leamy, 1982; Holt, 1989) and on electron-stimulated desorption (ESD) effects (Knotek, 1984; Pantano and Madey, 1981). With a 15-kV, 100-pA

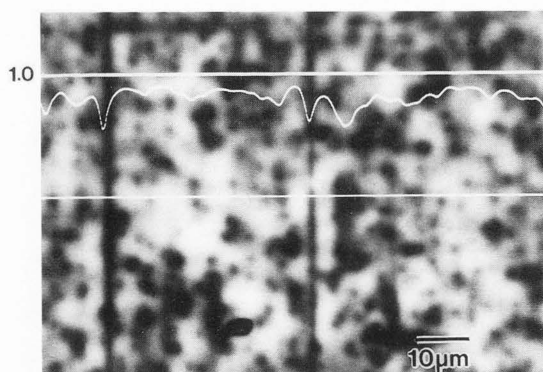

Figure 3. EBIC line scan superimposed on an EBIC map of the defects in an epilayer of GaAs on a silicon substrate. The top line is the 100% electron beam quantum efficiency reference line per equation 1. The bottom line is both the position of the line scan and the zero beam current reference line. The middle line is the EBIC linescan indicating the actual current loss in a defect area relative to 100% collection. Bar = 10 μm.

beam in Si, the injection levels are 10^{23} pairs/cm^3/sec. In addition, ESD processes scale directly with the charge density (*ibid.*). In an earlier work, for example, the case was made that even with a 100-A, 20-kV, 50-pA beam, the electron beam was desorbing oxygen from polycrystalline $CuInSe_2$, thereby locally type-converting it from p-type to n-type (Matson *et al.*, 1989). Using 5-kV, 60-nA, 5-μm diameter beam conditions to approximate the same charge density conditions of the SEM/EBIC work, this effect was corroborated by Auger electron spectroscopy (*ibid.*). These observations suggest the use of higher E_b and lower I_b in CCM be considered, consistent with resolution requirements.

In more practical terms, the sample mounting and connections and the detection of the CCM signal are aided considerably by an EBIC stage similar to that in Figure 4, which proves itself invaluable under routine use, as the device can be loaded and tested on a curve tracer before insertion into the SEM and can be made to insert directly into a corresponding connector inside the SEM which is then connected, via vacuum feedthrough, to the amplifier and SEM display circuitry. This idea can easily be extended to many other SEM stage arrangements (see Matson, 1983). The real utility is in the ability to make quick contact to devices of a variety of configurations. Many experimental devices are two terminal. By connecting half of the probe positions together for one side of the device and the other half together for the other side of the device, a number of positions for the tungsten probes are available, allowing for a good bit of versatility. The variable positioning of

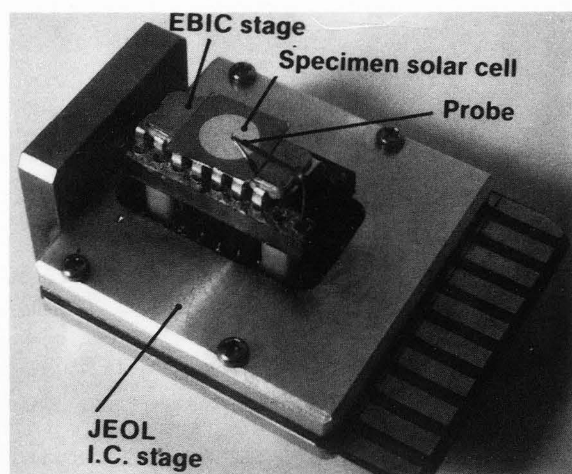

Figure 4. An extension of an SEM IC stage commercially available from JEOL. The idea can easily be extended to many other SEM stage arrangements. This includes a 50° tilt mount to facilitate cross-section work. The real utility is in the ability to make quick contact to devices of a variety of configurations.

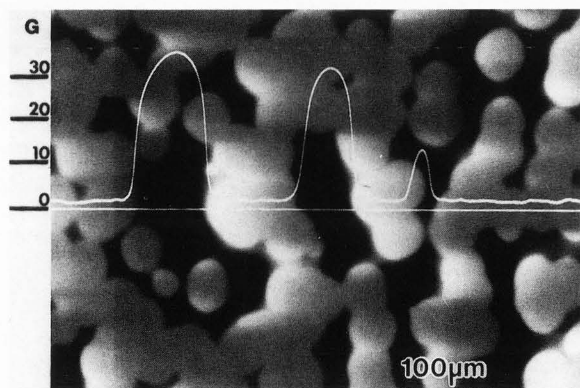

Figure 5. Electron-beam-induced conductivity micrograph of high-dose nitrogen-implanted silicon. The scale of charge multiplication gain to the left refers to the EBIC line scan indicating variations in the conductivity of the material (the polarity of the linescan is reversed with respect to that of the image due to an unintended phase difference between the lock-in amplifier used with the EBIC linescan versus the amplifier used for the image). Bar = 100 μm.

---

the tungsten probes in height also allows for variable pressure. Via a feedthrough, the signal then can be fed to an amplifier switching box where the signal can then be readily forwarded to a variety of amplifiers, depending on the device and purpose at hand. For true EBIC, the amplifiers need to be high-gain, low-input impedance, low-noise, large-bandwidth amplifiers (see Lesniak *et al.*, 1984), with lock-in amplification being ideal for low-level-signal linescans.

The "detector" is important as well. One should choose small-area devices (to cut down on capacitive effects) and optimal contacting, both for minimizing the overall time constant of the system (Holt, 1974). If it is not already a p/n device, but semiconductor material under investigation, it can be quite simple to form a Schottky barrier device with the use of just silver paint for a back contact. The aforementioned ~200 Å of Au often suffices for a Schottky barrier and also allows for follow-on cathodoluminescence (CL) characterization, as the light can escape through such a thin layer of Au. Again, the advantage of the large charge multiplication of the technique allows for relatively inefficient (weak) devices to work well for characterizing nonuniformities in the material if CL is inconvenient.

Applications

In terms of applications of CCM, perhaps the first distinction to be made is between planar and junction (or cross-sectional) EBIC configurations. Figure 1 and 2 demonstrate planar EBIC, where the beam is normal to the plane of the junction. It is often useful to include an EBIC linescan superimposed on the EBIC image in order to scale the significance of the EBIC contrast, as in Figure 3. Otherwise, with the use of differential amplification, the actual seriousness of the defects for the device can be quite uncertain to the reader.

A variation of this technique is electron-beam-induced conductivity. In general, when a high energy electron enters a semiconductor or an insulator, there is a significant increase in the local conductivity due to the creation of excess e/h pairs that are free to migrate. Termed β-conductivity, the phenomenon is directly analogous to photoconductivity (Ehrenberg and Gibbons, 1981). An example of this is that of high-dose nitrogen implantation of silicon with the intention of creating a uniform insulating layer of Si_3N_4 (Figure 5). In this case, although dielectric breakdown in the devices made from the insulating layer was observed, the investigators could not determine in what manner the material was breaking down (Kwor *et al.*, 1989). Examining the device in the conventional CCM configuration (that is, without the use of the biasing common to the electron-beam-induced conductivity technique), the variation in conductivity shown in Figure 5 became apparent. The scale to the left of the micrograph is for the gain which is defined differently than in equation (2). Here the gain signifies a charge multiplication defined in terms of multiples of I_b. Therefore, a gain of 30 signifies an EBIC value 30 times greater than the I_b. The scale of

charge multiplication gain to the left refers to the EBIC linescan, indicating variations in the conductivity of the material (the polarity of the linescan is reversed with respect to that of the image due to a phase difference between the lock-in amplifier used with the EBIC linescan versus the amplifier used for the image).

This observed charge multiplication and collection suggests the existence of a weak field to account for the charge separation required by the collection of such gain. One possible explanation of this observed effect of charge separation without an actual barrier, or p-n junction, being present is that charge may be trapped in a surface oxide, or in an insulating layer, and functioning as an effective space-charge layer at the crystal/oxide interface, thereby affecting charge separation and collection. The variations in these properties were interpreted as variations in the conducting properties of the Si_3N_4 layer (Kwor *et al.*, 1989).

In contrast to planar EBIC, "junction" (or cross-sectional) EBIC (JEBIC), depicted in Figure 6, requires that the beam be coplanar with the junction. Following Figure 6, the electron beam is scanned in a line normal to the device junction in cross-section (a). Shown is the corresponding energy band diagram for a heterojunction device (b), the electric field of the space charge region (c), and the resulting EBIC line scan or charge collection efficiency profile (d). It can be used to determine the location of the junction in the device, the spatial uniformity of the junction (especially, in experimental polycrystalline devices) and the space-charge region, and can also be used to determine minority-carrier diffusion lengths. As an example, Figure 7 shows a SEI of a thin-film poly-crystalline $CdS/CuInSe_2$ photovoltaic device with a corresponding Y (or amplitude) modulated EBIC map of the same area to its right. Note the considerable variation in junction location, variations in what could be taken as the space-charge region width, and minority-carrier diffusion lengths due to small-scale variations in the defect chemistry of the material (which is what determines the electronic properties of this material) (Matson *et al.*, 1986) (a close comparison of SEIs and carefully superimposed EBIC line scans shows that the variations in the EBIC profile are only secondarily due to topography). The use of CCM for diffusion length measurements has been dealt with extensively in the CCM/EBIC literature [see, for example, Leamy (1982), Wu and Wittry (1978), Donolato (1983), Shea *et al.* (1978), Ioannou and Dimitriadis (1982), or Bell and Hanoka (1982)].

An extension of this technique, and our last example, is the location of back-to-back junctions through the use of bias. Figure 8 is from molecular beam epitaxy (MBE) GaAs grown on a Ge substrate. Whereas the junction near the outer surface of the GaAs was expected, the junction induced in the Ge, via autodoping of the Ge by both Ga and As, was not (Tobin *et al.*, 1988). Although the second junction was not in

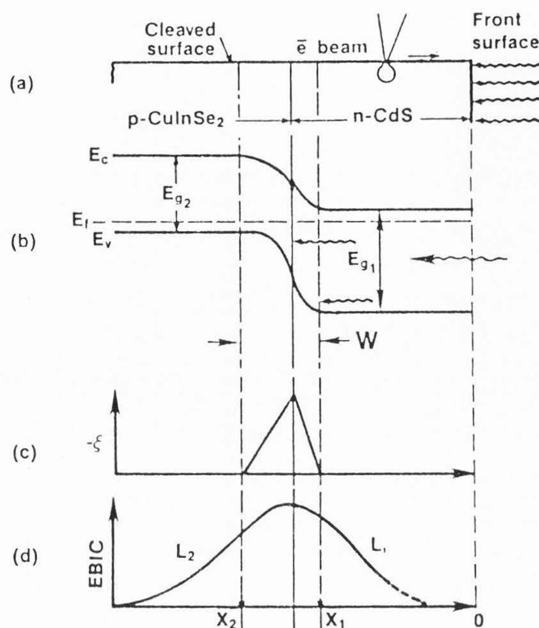

Figure 6. Diagram of junction EBIC technique with $CdS/CuInSe_2$, as an example. The electron beam is scanned in a line normal to the device junction in cross-section (**a**). Shown is the corresponding energy band diagram for heterojunction device (**b**), the electric field of the space charge region (**c**), and the resulting EBIC line scan or charge collection efficiency profile (**d**).

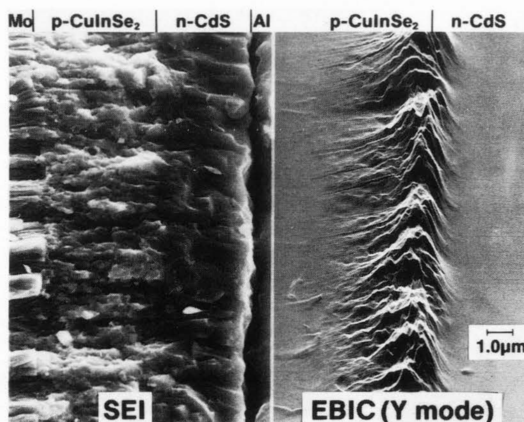

Figure 7. Comparison of a SEI and Y-modulated EBIC image of the same area of a cross section of a thin-film, polycrystalline $CdS/CuInSe_2$ device. Bar = 1.0 μm.

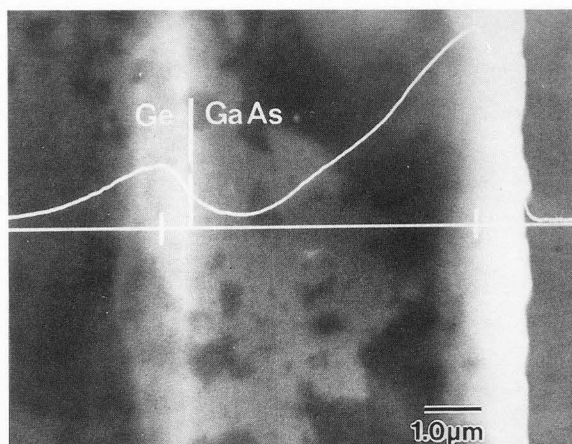

Figure 8. Biased EBIC linescan of epilayer of GaAs on Ge substrate, illustrating the use of bias to detect the existence and location of a second junction in the Ge substrate arising from Ga and As autodoping. Bar = 1.0 μm.

---

evidence with conventional JEBIC, it became evident with applied bias to balance the counter currents. Due to the large (mA level) currents induced by biasing in comparison to the CCM currents (nA), care and lock-in detection techniques were necessary.

Conclusions

In this relatively short treatment of CCM theory and the use of CCM in electronic (primarily photovoltaic) materials and device research, the reader has been introduced to both the ease of deployment and a variety of applications of the CCM/EBIC techniques. If not directly relevant to the reader's research efforts, the hope is that analogous applications will become evident in indirectly related fields of research.

References

Bell RO, Hanoka JI (1982) Improved spatial resolution diffusion length measurements in imperfect silicon. J. Appl. Phys. **53**, 1741-1744.

Donolato C (1983) Evaluation of diffusion lengths and surface recombination velocitites from electron-beam-induced current scans. Appl. Phys. Lett. **43**, 120-122.

Ehrenberg W, Gibbons DJ (1981) Electron-Bombardment-Induced Conductivity and Its Applications. Academic Press, London, 80-122.

Holt DB (1974) Quantitative conductance mode scanning electron microscopy. In: Quantitative Scanning Electron Microscopy. Holt DB, Muir DB, Grant PR, Boswarva IM (eds.). Academic Press, London, 213-286.

Holt DB (1989) The conductive mode. In: SEM Microcharacterization of Semiconductors. Holt DB, Joy DC (eds.). Academic Press, London, 241-338.

Ioannou DE, Dimitriadis CA (1982) A SEM-EBIC minority carrier diffusion length measurement technique. IEEE Trans. Elec. Dev. **ED-29**, 445-450.

Knotek ML (1984) Stimulated desorption from surfaces. Phys. Today **37**(9), 24-32.

Kwor R, Matson RJ, Al-Jassim MM, Polchlopek S, Hemment PL, Reeson KJ (1989) EBIC study of silicon on insulator structures formed by high dose nitrogen implantation. J. Electrochemical Society **136**, 876-878.

Leamy HJ (1982) Charge collection scanning electron microscopy. J. Appl. Phys. **53**(6), R51-R80.

Lesniak M, Unvala BA, Holt DB (1984) An improved detection system for electrical microcharacterization in a scanning electron microscope. J. Microscopy, **135**, 255-274.

Matson RJ (1983) Modifications to, and applications of, the JEOL JSM 35c for EBIC analysis of photovoltaic devices. Japanese Electron-Optics Laboratory News. **21**E(2), 10-13 (contact JEOL U.S.A. or author for copy).

Matson RJ, Noufi R, Ahrenkiel RK, Powell RC, Cahen D (1986) EBIC investigations of junction activity and the role of oxygen in CdS/$CuInSe_2$ devices. Solar Cells, **16**, 495-519.

Matson RJ, Kazmerski LL, Noufi R, Cahen D (1989) Electron-stimulated desorption of oxygen from, and the subsequent type conversion of, thin film p-$CuInSe_2$. J. Vac. Sci. Technol. **A7**(2), 230-233.

Pantano CG, Madey TE (1981) Electron beam damage in Auger electron spectroscopy. Appl. Surf. Sci. **7**, 115-141.

Sieber B (1991) Origin of recombination at extended defects: EBIC contrast experiments and theory on dislocations in GaAs. Solid State Phenomena, **19**, **20**, 353-366.

Shea SP, Partain LD, Warter PJ (1978) Resolution limits of the EBIC technique in the determination of diffusion lengths in semiconductors. Scanning Electron Microscopy **1978**;1, 435-444.

Tobin SP, Vernon SM, Bajgar C, Haven VE, Geoffrey LM, Hart RE, Emery KA, Matson RJ (1988) High efficiency GaAs/Ge monolithic tandem solar cells. In: Proc. 20th IEEE Photovoltaics Specialists Conference (Las Vegas, NV). IEEE, New York, 405-412.

Wu CJ, Wittry DB (1978) Investigations of minority-carrier diffusion lengths by electron bombardment of Schottky barriers. J. Appl. Phys. **49**, 2827-2836.

Discussion with Reviewers

L. Balk: You suggest the use of high E_b and low I_b for CCM. Is this a common rule or should the I_b and E_b be chosen as low as possible to obtain the optimal spatial resolution?

Author: The suggestion to use high E_b and low I_b was only with respect to minimizing the carrier injection density to avoid high injection conditions in the device. However, more often one chooses low E_b for smaller scattering volumes and, therefore, better resolution. Also, in general, the lowest I_b values (consistent with satisfactory S/N conditions) are always preferred both for injection rates and any beam induced effects (see Matson *et al.*, 1989).

L. Balk: You show a superimposed EBIC linescan on the EBIC image to scale (Figure 3) and estimate the seriousness of the defects. Can you give a quantitative relationship between the EBIC contrast and the seriousness of a defect?

Author: As you well know, there has been extensive modelling done in the area of quantitative EBIC evaluation of defects (Donolato, 1979; Jakubowicz, 1985; Donolato and Klann, 1980; Hanoka and Bell, 1981; Sieber, 1991 — to name a few). It is a complex phenomenon and depends on the depth and type of defects, the E_b, and so on. However, a useful, albeit rough, approximation of current lost to defects can be achieved by effectively estimating the integrated current losses over a single EBIC linescan or an entire image with respect to the peak response of the device. This can be used to measure relative improvements due to defect passivation techniques. We have compared such current loss values with the relative changes in the device short circuit current (I_{sc}) before and after defect passivation techniques. For example, integrating current losses with respect to the peak current in Figure 9 for the before, and after, passivation cases gives a good estimate of the effects of passivation as compared with values for the whole device I_{sc}. The image consists of EBIC linescans superimposed on an EBIC image of an area before (upper) and after (lower) hydrogen passivated. Although both EBIC linescans are with respect to the horizontal reference line, the top linescan is from the passivated area and the lower linescan is from the non-passivated area. Although possible to achieve, a more rigorous quantification in each case is probably much more effort than what is warranted.

D. Holt: We have begun using CCM to look at bias-induced p-n junctions in $CuInSe_2$ in cooperation with D. Cahen, with whom you also co-operated; can you give any guidance concerning the role of electron-stimulated desorption (ESD) in CCM? Does the type conversion that you mention create a new p-n junction and additional bright areas? How long does it take? Is it temperature dependent?

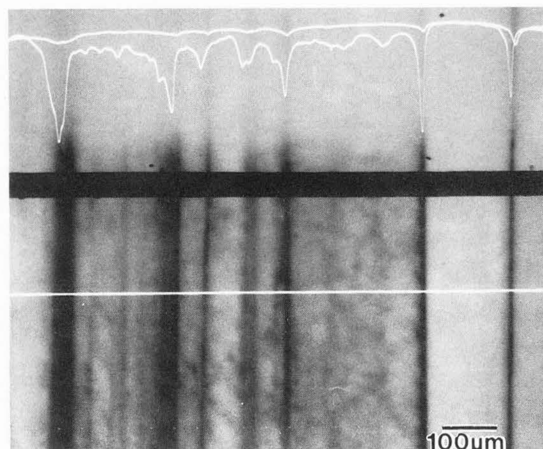

Figure 9. Comparison of passivation effects on defects and grain boundaries in polycrystalline Si by hydrogenation. The image consists of EBIC linescans superimposed on an EBIC image of an area of a device before (upper portion) and after (lower portion) hydrogen passivated. Although both EBIC linescans are with respect to the horizontal reference line, the top linescan is from the passivated area and the lower linescan is from the non-passivated area. Bar = 100 μm.

Author: The work by Cahen and co-workers you are referring to involves the local type conversion of single crystal $CuInSe_2$ (CIS) via the application of voltage bias. The only ESD (or electron stimulated type conversion) in CIS that I have observed has been in poly-crystalline, thin film CIS. As such, I will have to address your questions with respect to the thin film case. Referring to Matson *et al.* 1986 and 1989 and Figure 10, we see in (a) an initial (i) and a final (f) EBIC linescan (the structure is evident both from the labeling and the columnar structure of the Mo back contact on the substrate, the ~3.0-3.5-μm thick and almost granular structure of the CIS and the ~3.0-3.5-μm thick and columnar structure of the CdS. The black ticks indicate the position of the metallurgical junction). The initial EBIC linescan is a "virgin" linescan (i.e., without previous exposure to the e-beam). The final linescan (f) is the linescan after a number of successive EBIC linescans have "shifted" and, finally, stabilized. This 1 μm shift of the EBIC peak represents a local type conversion of the material and, therefore, a new junction location. Viewed as an image, the corresponding "bright spot", or locus of increased collection, will have moved (just in the area effected). Depending on the particular sample,

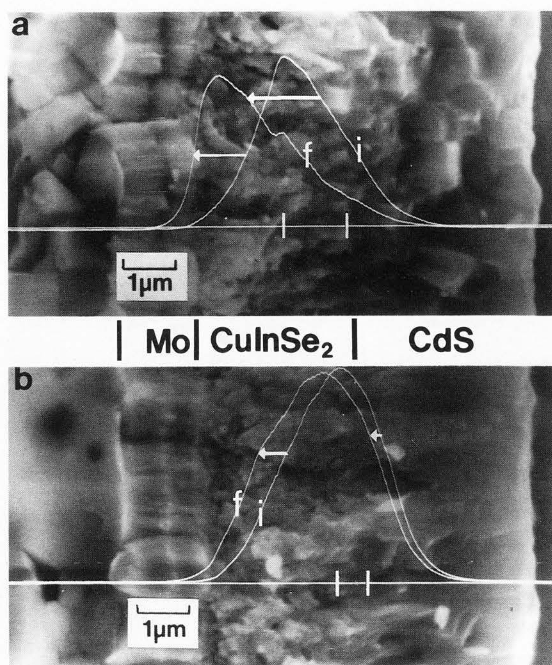

Figure 10. Comparison of initial (i) and final (f) EBIC linescans for a CdS/$CuInSe_2$(CIS) device before heat treatment (**a**) and after heat treatment (225°C, O_2, 30 min). (**b**) The structure is evident both from the labeling and the columnar structure of the Mo back contact on the substrate, the ~3.0-3.5-μm thick and almost granular structure of the CIS and the ~3.0-3.5-μm thick and columnar structure of the CdS. The black ticks indicate the position of the metallurgical junction. (From Matson, *et al.*, 1986) Bar = 1.0 μm.

---

deposition technique, post-deposition treatment, the E_b and I_b, and scan rate, such a shift as in (a) can take anywhere from a few seconds to a few minutes. Basically, the charge density per time determines if, and at what rate, the type conversion occurs. In terms of temperature dependence, we have observed temperature dependent behavior down to 80°K, but have not performed any systematic investigation on which to base a general statement (Noufi *et al.*, 1988). In general, the resulting electron beam induced local type conversion is much more dramatic in the as-deposited material before the post deposition heat/oxygen treatment than after it. Evident in Figure 10b, the post-deposition, heat-treatment (in air) case, we see both that the junction has moved closer to the CdS/CIS heteroface, or metallurgical junction, and that the "EBIC shift" is much less. More ample evidence for believing that the e-beam is desorbing oxygen, resulting in type conversion, is given in the above references.

D. Holt: How general is electron-stimulated desorption?

Author: The parameter of interest in ESD is the critical dose, or the minimum dose of electrons required for beam effects to be detected. The critical dose for many practical samples is on the order of 1 to 10 mc/cm^2, and the threshold for many ESD processes is between 10 and 40 eV (Pantano and Madey, 1981). Hence with a common set of SEM beam parameter values such as 20 kV, 50 pA, and 100 Å diameter, we have a current density of 60 A/cm^2, a 0.01-μm beam diameter, a 1-μm/second linescan rate (slow scan at 10 kX mag). Treating a 1-μm linescan as a succession of 0.01-μm steps, the exposed material in the EBIC/SEM experiment is subject to a charge dose of 60 mc/cm^2 per pass of the electron beam, while being bombarded by 20-keV electrons. This is 60 to 600 times greater than the aforementioned critical dose value. The criteria for the stability of ionically bonded solids in an ionizing environment, such as in an SEM, have been provided by Knotek and Feibelman (1978, 1979). Lacking the appropriate forum to pursue your question, I think it is fair to say that ESD phenomena are probably quite common in our SEM work but go largely undetected.

D. Holt: Is your use of the term gain, G, in Figure 5 the same as Joy's usage, namely, g = I_{cc}/I_b, i.e., $\eta_{cc}G$? Where are the contacts in this configuration ?

Author: As in David Joy's usage, it is no more than I_{cc}/I_b. The contacts are top and bottom, i.e., with the back surface of the Si substrate as one contact and a probe on top to the Si_3N_4 layer.

S. Myhajlenko: Has the author considered the possibility of strain effects associated with the nitrogen implantation or the silicon nitride itself being responsible for the small EBIC gain observed in Figure 5?

Author: In view of the work referenced in your next question, I believe it is a good possibility.

S. Myhajlenko: What are the author's thoughts on the applicability of remote contact EBIC (REBIC) to semiconductor process characterization? [see, e.g., Bubulac and Tennant (1988)].

Author: I think it may often prove worthwhile to try this simple technique whenever there is any reason to believe that charge-separating defects [i.e., any fields that might exist due to inclusions, damage, dislocations, strain, p-n junctions (due to actual doping, autodoping or a contact that is actually functioning as a weak Schottky barrier)] may be present.

Additional References

Bubulac LO, Tennant WE (1988) Observation of

charge-separating defects in HgCdTe using remote contact electron beam induced current. Appl. Phys. Lett. **52**, 1255-1257.

Donolato C (1979) Contrast formation in SEM charge-collection images of semiconductor defects. Scanning Electron Microscopy **1979**;I, 257-266.

Donolato C, Klann H (1980) Computer simulation of SEM electron beam induced current images of dislocations and stacking faults. J. Appl. Phys. **51**, 1624-1633.

Hanoka JI, Bell RO (1981) Electron-beam-induced currents in semiconductors. In: Annual Review of Materials Science, **11**. Pub. Annual Reviews, Palo Alto, CA, 353-380.

Jakubowicz A (1985) On the theory of electron-beam-induced current contrast defects in semiconductors. J. Appl. Phys. **57**, 1194-1199.

Knotek ML, Feibelman PJ (1978) Ion desorption by core-hole Auger decay. Phys. Rev . Lett. **40**, 964-967.

Knotek ML, Feibelman PJ (1979) Stability of ionically bonded surfaces in ionizing environments. Surface Science **90**(1), 78-90.

Noufi R, Ramanathan V, Matson RJ (1988) Low-temperature characteristics of $CdS/CuInSe_2$ diodes. Solar Cells, **24**, 11-17.